Computational studies of current blockades by αHL adducts

1 Model preparation

Because the thiol-disulfide interchange reaction occurs only within the β barrel of the αHL nanopores, a minimal β barrel model was constructed.[1] In this model, residues Glu-111 to Asn-123, which are in or close to the β barrel region were kept, and all residues outside the β barrel region were deleted. To further reduce model complexity, all membrane-facing sidechains were removed. Six systems, αHL-TNB or αHL-DTT adducts at positions 113, 117 or 121, were prepared. Force field parameters for the cysteine residues carrying TNB or DTT molecules were obtained from the GAFF force field.[2,3] For the modified residues, partial charges were determined with the Restrained Electrostatic Potential (RESP) method at the HF/6-31G* level using Gaussian16[4] and ANTECHAMBER.[2,3]

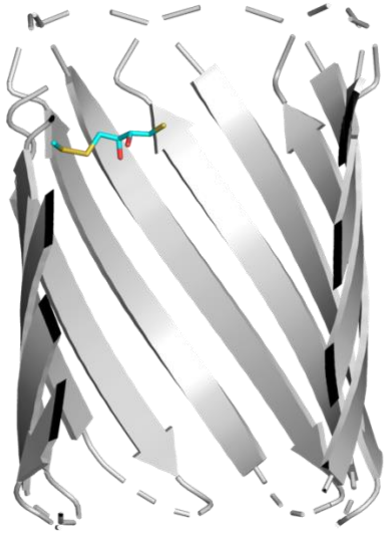

Figure S1. The model pore system setup. A αHL-DTT adduct (cyan) at position 113 in truncated pore is (grey) shown as an example.

2 Molecular dynamics simulation protocol

Molecular dynamics (MD) simulations were performed with GROMACS (v2019.2).[5] For each system, the nanopore was modeled with the AMBER99SB-ILDN force field and inserted into a cubic box of TIP3P water molecules.[6,7] The system was neutralized and 0.15 M NaCl was added. The system was energy minimized using the steepest descent algorithm until the maximum force was below 1000 kJ mol^{-1} nm^{-1}. A positional restraint of 1000 kJ mol^{-1} nm^2 was subsequently applied on the protein backbone atoms. Three independent runs were performed with random initial velocities generated according to the Maxwell–Boltzmann distribution at 298 K. The system was equilibrated under a constant volume and temperature (NVT) ensemble at 298 K (100 ps, 2 fs timestep), followed by equilibration under a constant pressure and temperature (NPT) ensemble at 1 bar and 298 K (100 ps, 2 fs timestep). Production simulations were performed using the NPT ensemble at 1 bar and 298 K (200 ns, 2 fs timestep). An electric field of 0.008 V nm^{-1} (equivalent to ~50 mV across the membrane) was applied in the Z direction across the simulation box. The temperature of the system was maintained at 298 K using the V-rescale thermostat.[8] Pressure was controlled by the Parrinello-Rahman barostat at 1.0 bar, with an isothermal compressibility of 4.5×10^{-5} bar^{-1}.[9] All simulations were performed with three-dimensional periodic boundary conditions. Long-range electrostatics was described with the Particle Mesh Ewald (PME) algorithm.[10,11] All bond lengths involving hydrogen atoms were constrained using the LINCS algorithm.[12] Structures and input files are available on GitHub at https://github.com/duartegroup/Current-blockade-in-nanopore.

3 Current blockade and spatial blockade

As shown in Figure 2e in the main text, the percentage current blockade of αHL-TNB (I_{TNB}%) and αHL-DTT (I_{DTT}%) adducts varied at the six positions tested along the β barrel. I_{TNB}% showed a gradual decrease from position 113 to 123, whereas I_{DTT}% exhibited a U-shaped behavior with a minimum at position 119. This was accompanied by a switch in relative magnitude (i.e., I_{TNB}% > I_{DTT}% at positions 113-117; I_{TNB}% = I_{DTT}% at positions 119 and 121; I_{TNB}% < I_{DTT}% at position 123). This shows that current blockade by molecules within an αHL pore is not simply determined by molecular mass.

Spatial blockades of the αHL-TNB or αHL-DTT adducts at Cys-113, Cys-117, and Cys-121, defined as the end-to-end distance of the adduct divided by the radius of the unreacted pores at the cysteine position, were calculated over 600 ns of cumulative MD simulations. The spatial blockade was calculated as the end-to-end distance of an adduct divided by the radius of the unreacted pore at the cysteine positions in the unreacted pores (r_{113} = 5.8 Å, r_{117} = 5.5 Å, r_{121} = 6.4 Å) and labelled as d_{TNB}% and d_{DTT}%. The radius of the unreacted pore at each position was calculated using the HOLE program.[13,14] A positive linear correlation was found between Δd% (d_{TNB}% – d_{DTT}%) and ΔI% (I_{TNB}% – I_{DTT}%) (R^2 = 0.98, Figure S2c), suggesting a strong correlation between the relative spatial blockade and the relative current blockade.

The αHL-DTT adducts have multiple conformational states, categorized by the end-to-end distances of the adducts (d_{EE}) (Figure S3). The conformations of the αHL-DTT adducts were predominantly stabilized by hydrogen bonding (HB) interactions between suitably oriented hydroxyl groups of DTT and neighboring residues. For example, at position 113, a HB interaction between a hydroxyl group of DTT and Thr-145 on the adjacent strand (occupancy = 24%) resulted in an extended conformation of αHL-DTT (d_{EE} = 10 Å), whereas a HB interaction with Glu-111 on the same strand (occupancy = 10%) led to a folded conformation (d_{EE} = 4.9 Å). At positions 117 and 121, the αHL-DTT adduct adopted an extended conformation with both hydroxyl groups pointing towards the water-filled channel (d_{EE} = 7.5 Å) with HB interactions with the protein backbone on the adjacent strand: Ser-141 at position 117 (occupancy = 5%), and Gly-122 at position 121 (occupancy = 10%). In comparison, the αHL-TNB adducts had only one major state (Figure S4). This was attributed to the rigidity of the benzene ring, resulting in conformational flexibility mainly coming from the cysteine side chain. A HB interaction was found between the αHL-TNB adduct at position 113 and Thr-145 on the adjacent strand (occupancy = 18%), while no significant HB interactions were found for adducts at positions 117 and 121.

A

Cysteine position	Experimental (I_{block}%)		Computational (d_{EE}%)	
	I_{TNB}%	I_{DTT}%	d_{TNB}%	d_{DTT}%
Cys-113	6.53 ± 0.18	4.65 ± 0.24	15.3 ± 0.1	13.2 ± 0.7
Cys-115	5.08 ± 0.15	3.06 ± 0.12	/	/
Cys-117	3.90 ± 0.23	2.71 ± 0.15	15.3 ± 0.1	13.9 ± 0.3
Cys-119	2.84 ± 0.15	2.57 ± 0.14	/	/
Cys-121	2.60 ± 0.07	2.80 ± 0.19	12.3 ± 0.1	13.4 ± 0.2
Cys-123	2.10 ± 0.12	3.48 ± 0.12	/	/

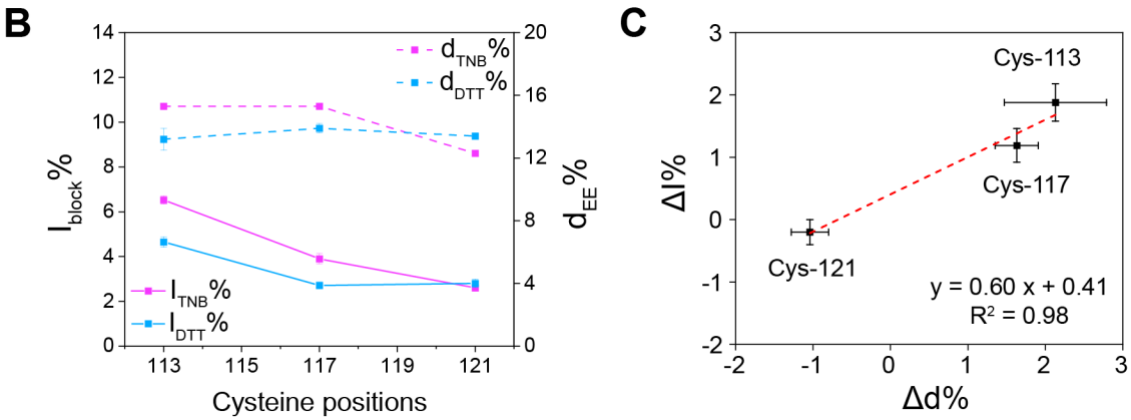

Figure S2. Relationship between current blockade and spatial blockade of the adducts. (A) Summary of percentage current blockades (I_{block}%: I_{TNB}% and I_{DTT}%) and end-to-end distances of the αHL-TNB and αHL-DTT adducts at positions 113, 117 and 121 (d_{EE}%: d_{TNB}% and d_{DTT}%) as a percentage of the radius at the cysteine position of the unreacted pore. For each adduct, the values were calculated over 600 ns of cumulative MD simulations. (B) Comparison between I_{block}% (solid line) and d_{EE}% (dashed line). (C) A linear correlation between Δd% (d_{TNB}% – d_{DTT}%) and ΔI% (I_{TNB}% – I_{DTT}%).

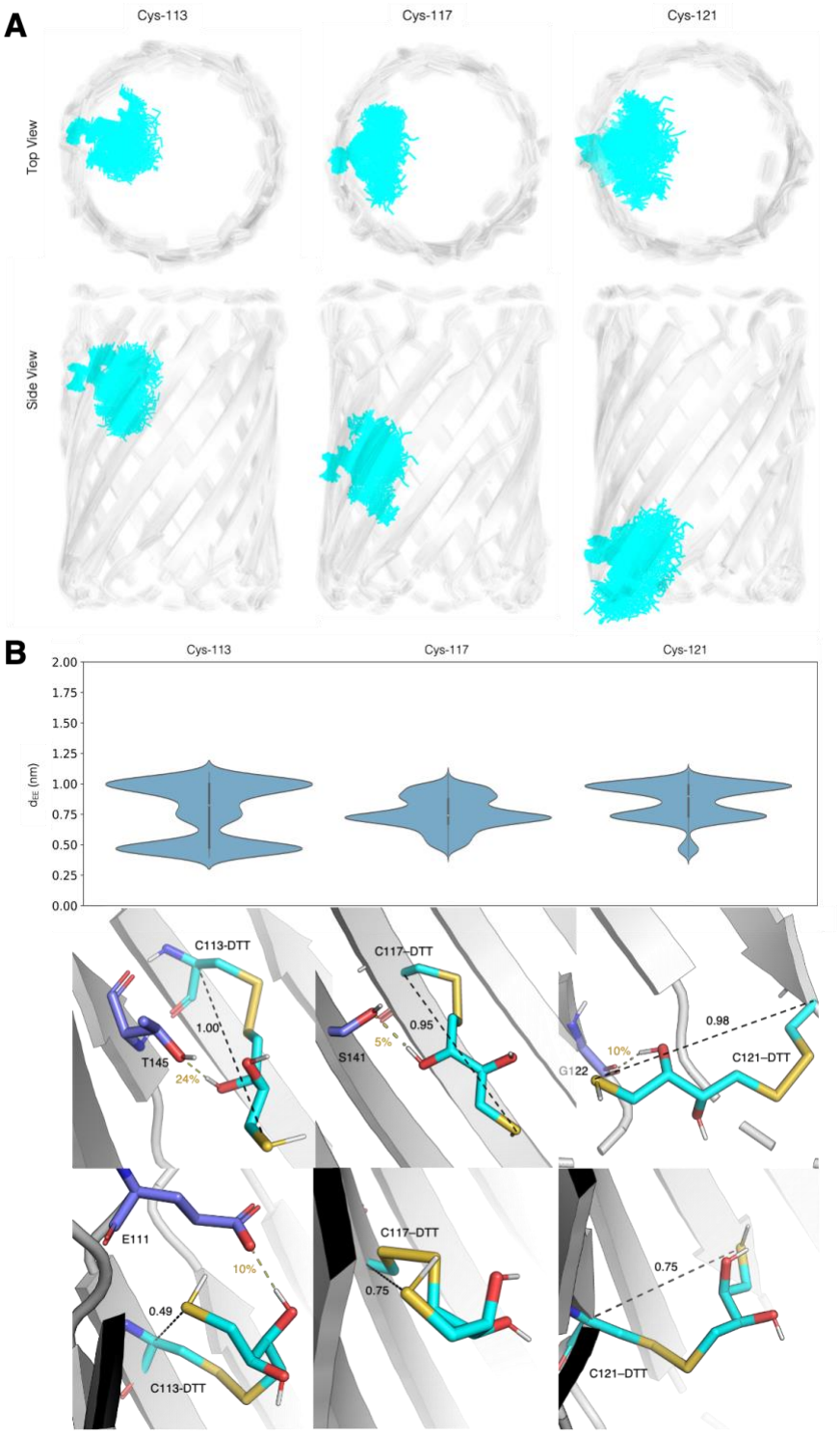

Figure S3. Conformations of the αHL-DTT adducts at positions 113, 117 and 121. (A) Overlap of all conformations of the αHL-DTT adducts (cyan) over 600 ns of cumulative MD simulations at position 113, 117 and 121 respectively. (B) Top: Probability density of the end-to-end distance (d_{EE}) of an αHL-DTT adduct, calculated as the distance between the C_α atom of the cysteine residue and the terminal sulfur atom of the αHL-DTT adduct at position 113, 117 and 121 respectively. Bottom: Two most populated conformations of the αHL-DTT adducts (cyan). d_{EE} is indicated with a black dashed line. Hydrogen bonding to a neighboring residue (purple) and its occupancy is indicated in yellow.

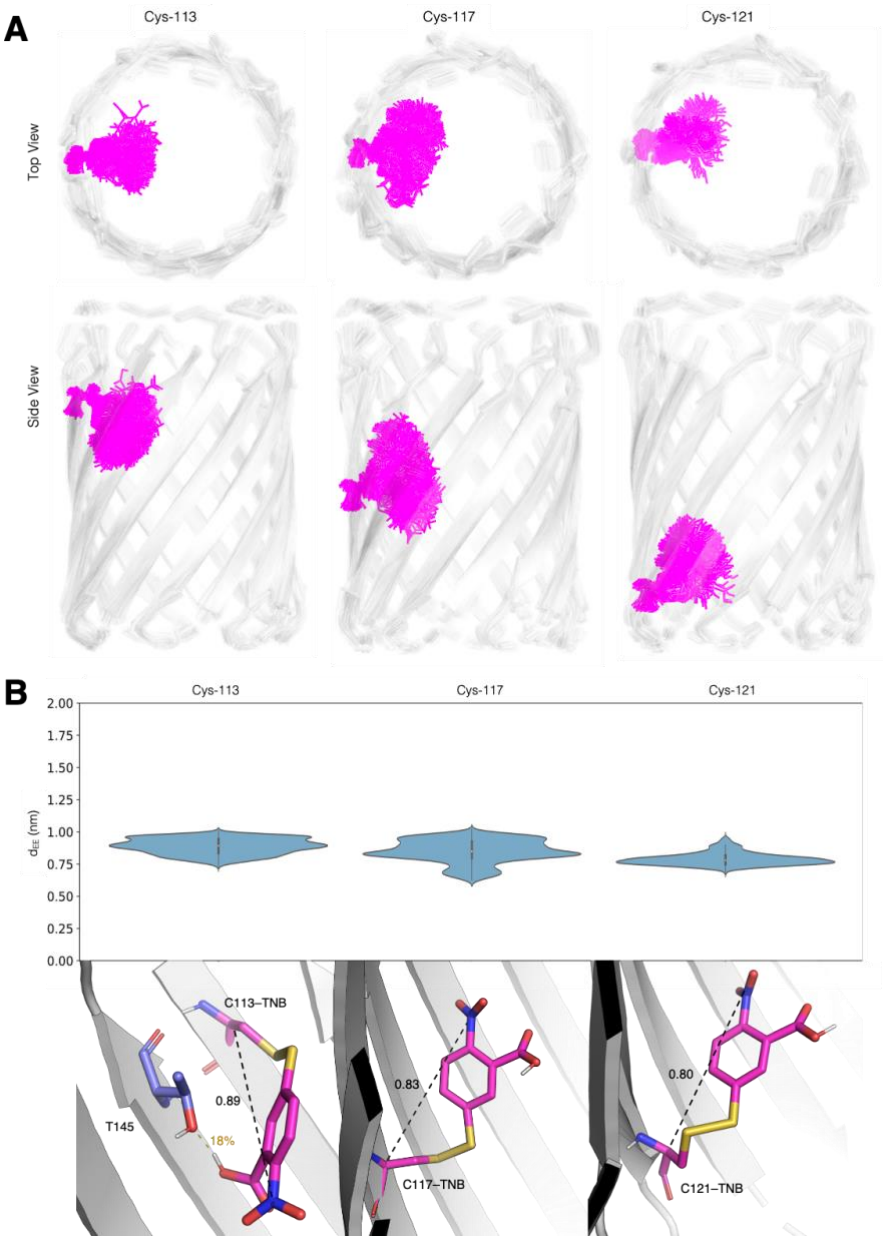

Figure S4. Conformations of the αHL-TNB adducts at positions 113, 117 and 121. (A) Overlap of all conformations of the αHL-TNB adducts (magenta) over 600 ns of cumulative MD simulations at position 113, 117 and 121 respectively. (B) Top: Probability density of the end-to-end distance (d_{EE}) of an αHL-TNB adduct, calculated as the distance between the C_α atom of cysteine residue and the terminal nitrogen atom of the αHL-TNB adduct at position 113, 117 and 121 respectively. Bottom: The most populated conformation of the αHL-TNB adducts (magenta). d_{EE} is indicated with a black dash. Hydrogen bonding to a neighboring amino acid (purple) and its occupancy is indicated in yellow.

References

[1] P. J. Bond, A. T. Guy, A. J. Heron, H. Bayley, S. Khalid, *Biochemistry* **2011**, *50*, 3777–3783.

[2] J. Wang, W. Wang, P. A. Kollman, D. A. Case, *J. Mol. Graph. Model.* **2006**, *25*, 247–260.

[3] J. Wang, R. M. Wolf, J. W. Caldwell, P. A. Kollman, D. A. Case, *J. Comput. Chem.* **2004**, *25*, 1157–1174.

[4] M. J. Frisch, G. W. Trucks, H. B. Schlegel, G. E. Scuseria, M. a. Robb, J. R. Cheeseman, G. Scalmani, V. Barone, G. a. Petersson, H. Nakatsuji, X. Li, M. Caricato, a. V. Marenich, J. Bloino, B. G. Janesko, R. Gomperts, B. Mennucci, H. P. Hratchian, J. V. Ortiz, a. F. Izmaylov, J. L. Sonnenberg, Williams, F. Ding, F. Lipparini, F. Egidi, J. Goings, B. Peng, A. Petrone, T. Henderson, D. Ranasinghe, V. G. Zakrzewski, J. Gao, N. Rega, G. Zheng, W. Liang, M. Hada, M. Ehara, K. Toyota, R. Fukuda, J. Hasegawa, M. Ishida, T. Nakajima, Y. Honda, O. Kitao, H. Nakai, T. Vreven, K. Throssell, J. a. Montgomery Jr., J. E. Peralta, F. Ogliaro, M. J. Bearpark, J. J. Heyd, E. N. Brothers, K. N. Kudin, V. N. Staroverov, T. a. Keith, R. Kobayashi, J. Normand, K. Raghavachari, a. P. Rendell, J. C. Burant, S. S. Iyengar, J. Tomasi, M. Cossi, J. M. Millam, M. Klene, C. Adamo, R. Cammi, J. W. Ochterski, R. L. Martin, K. Morokuma, O. Farkas, J. B. Foresman, D. J. Fox, **2016**, Gaussian 16, Revision C.01, Gaussian, Inc., Wallin.

[5] M. J. Abraham, T. Murtola, R. Schulz, S. Páll, J. C. Smith, B. Hess, E. Lindah, *SoftwareX* **2015**, *1–2*, 19–25.

[6] K. Lindorff-Larsen, S. Piana, K. Palmo, P. Maragakis, J. L. Klepeis, R. O. Dror, D. E. Shaw, *Proteins Struct. Funct. Bioinforma.* **2010**, *78*, 1950–1958.

[7] D. J. Price, C. L. Brooks, *J. Chem. Phys.* **2004**, *121*, 10096–10103.

[8] G. Bussi, D. Donadio, M. Parrinello, *J. Chem. Phys.* **2007**, *126*, DOI 10.1063/1.2408420.

[9] M. Parrinello, A. Rahman, *J. Appl. Phys.* **1981**, *52*, 7182–7190.

[10] T. Darden, D. York, L. Pedersen, *J. Chem. Phys.* **1998**, *98*, 10089.

[11] U. Essmann, L. Perera, M. L. Berkowitz, T. Darden, H. Lee, L. G. Pedersen, *J. Chem. Phys.* **1995**, *103*, 8577–8593.

[12] B. Hess, H. Bekker, H. J. C. Berendsen, J. G. E. M. Fraaije, *J. Comput. Chem.* **1997**, *18*, 1463–1472.

[13] O. S. Smart, J. M. Goodfellow, B. A. Wallace, *Biophys. J.* **1993**, *65*, 2455–2460.

[14] O. S. Smart, J. G. Neduvelil, X. Wang, B. A. Wallace, M. S. P. Sansom, *J. Mol. Graph.* **1996**, *14*, 354–360.